Journal of Applied Physics | METHOD | scitation.org/journal/jap

Quantitative analysis of boron–hydrogen pair dynamics by infrared absorption measurements at room temperature

Cite as: J. Appl. Phys. **131**, 235703 (2022); doi: 10.1063/5.0090965
Submitted: 10 March 2022 · Accepted: 19 May 2022 ·
Published Online: 21 June 2022

J. Simon,[a] A. Herguth, and G. Hahn

AFFILIATIONS

Department of Physics, University of Konstanz, 78457 Konstanz, Germany

[a]**Author to whom correspondence should be addressed:** jochen.simon@uni-konstanz.de

ABSTRACT

The ability of hydrogen quantification in crystalline silicon in concentrations as low as $10^{14}\,\mathrm{cm}^{-3}$ becomes fairly important in regard to hydrogen-related degradation phenomena in silicon devices generally and solar cells particularly. The method presented here allows for direct boron–hydrogen pair quantification and, therefore, allows inference on total hydrogen content. Hydrogen-rich amorphous silicon nitride was deposited on stripes of boron-doped float-zone silicon ($1\,\Omega\,\mathrm{cm}$), which were exposed to a rapid high temperature step to introduce relatively high amounts of hydrogen into the wafer. Infrared absorption spectra, which have been corrected for multiple reflection and free-carrier absorption, show absorption related to the boron–hydrogen stretching mode at $\tilde{\nu} = 1868\,\mathrm{cm}^{-1}$ with varying strengths during formation and subsequent dissociation of boron–hydrogen pairs triggered by annealing in the dark at 220 °C. Since the measurements were performed at room temperature, this method allows investigations with little effort and standard laboratory equipment. Furthermore, the change in free-carrier absorption (described by Drude's theory) is used to derive the change in hole concentration concurring with the formation and dissociation of boron–hydrogen pairs. The latter is found to fairly match not only the changing strength in absorption of the stretching mode, but also the change in hole concentration obtained by highly sensitive resistivity measurements. The comparison of stretching mode absorption strength and change in resistivity allows for a calibration of specific absorption, yielding a calibration factor A_{BH}. This calibration was performed with the absorption α $[A_{\mathrm{BH}}^{\alpha} = (4.2 \pm 0.3) \times 10^{15}\,\mathrm{cm}^{-1}]$ as well as with the quotient of absorption and wavenumber $\alpha/\tilde{\nu}$ $[A_{\mathrm{BH}}^{\alpha/\tilde{\nu}} = (7.8 \pm 0.6) \times 10^{18}\,\mathrm{cm}^{-2}]$.

© 2022 Author(s). All article content, except where otherwise noted, is licensed under a Creative Commons Attribution (CC BY) license (http://creativecommons.org/licenses/by/4.0/). https://doi.org/10.1063/5.0090965

I. INTRODUCTION

Hydrogen plays an important role in crystalline silicon for its ability to passivate and neutralize defects and impurities.[1] Despite its ability to passivate a multitude of recombination active defect species in silicon solar cells, hydrogen is also involved in the formation of recombination active defects in degradation phenomena, such as Light- and elevated Temperature-Induced Degradation (LeTID).[2–6] To clarify the dependence of the degradation on the hydrogen content, a precise quantification is necessary. Since typical hydrogen concentrations in silicon solar cells are only in the range of 10^{14}–$10^{15}\,\mathrm{cm}^{-3}$,[7–9] direct detection, e.g., by secondary ion mass spectrometry, is extremely difficult and often requires the use of less abundant deuterium. An alternative approach is indirect quantification by the tendency of hydrogen to form dopant-hydrogen pairs, thus changing bulk resistivity.[1,10] Although recent developments have shown that high precision can be achieved with this approach,[8,11] the change in resistivity is unspecific and not necessarily only due to the formation of dopant-hydrogen pairs.

The detection of local vibrational modes (LVMs) of specific binding configurations by means of infrared (IR) absorption spectroscopy gives direct access to the total dopant-hydrogen pair concentration and allows inference of total hydrogen concentration if the paired fraction is known sufficiently well. This has been done already with time-consuming measurements at cryogenic temperatures.[12,13] For the detection of light-element vibrational modes, typically, bulk concentrations of $10^{14}\,\mathrm{cm}^{-3}$ are required at cryogenic temperatures.[14]

© Author(s) 2022

Konstanzer Online-Publikations-System (KOPS)
URL: http://nbn-resolving.de/urn:nbn:de:bsz:352-2-zdiuqagv0k926

The approach presented in this contribution allows for direct boron–hydrogen quantification at room temperature. Measurements are performed on a single wafer in the longitudinal direction to increase absorption. Since the doping would freeze out at cryogenic temperatures, self-consistent comparisons to Drude absorption by free charge carriers can be made at room temperature only. Furthermore, the results are compared to resistivity measurements giving an accurate calibration factor between specific LVM absorption and binding concentration in the bulk.

II. BORON–HYDROGEN PAIR DYNAMICS

In crystalline silicon, atomic hydrogen H^+ (being predominantly positively charged in p-type silicon) can bind to dopant atoms, such as boron B^- (being negatively charged) in the form of overall neutral Coulombic pairs B^-H^+. However, hydrogen is predominantly present as neutral dimer H_{2A} (which refers to the interstitial ortho-H_2)[15] after a high temperature step followed by a sufficiently fast cool-down (quench),[16] and the following overall reactions occur in the dark in the temperature range below 290 °C investigated here:[9,17]

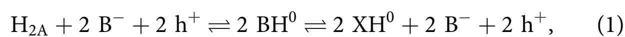

$$H_{2A} + 2\ B^- + 2\ h^+ \rightleftharpoons 2\ BH^0 \rightleftharpoons 2\ XH^0 + 2\ B^- + 2\ h^+, \qquad (1)$$

where the creation of atomic hydrogen H^+ from the neutral H_{2A} dimer consumes holes h^+, thus changing hole concentration p.[16] A subsequent dissociation [the right side of Eq. (1)] under the same experimental conditions, concurring with an increase in hole concentration, is interpreted as reactivation of boron and the formation of a so far unidentified neutral hydrogen complex XH^0 (which might be the dimer H_{2C} postulated by Voronkov and Falster[17]). However, effusion from the sample cannot be excluded as well.

Assuming first order reaction kinetics with constant reaction rates, thus neglecting the impact of changing hole concentration ($\Delta p \ll p$), the total BH pair concentration [BH] can be described by a double-exponential function (see Fig. 2),

$$[\mathrm{BH}] = A_1 \times \exp(-t/t_1) + A_2 \times \exp(-t/t_2) + A_\infty, \qquad (2)$$

with $t_{1,2}$ being effective time constants of BH pair formation and dissociation and $A_{1,2}$ being a measure of the concentration of BH pairs formed in the meantime. Note that the long-term value A_∞ is not necessarily zero but follows from the equilibrium reaction $BH^0 \rightleftharpoons XH^0$.

III. EXPERIMENTAL

For this experiment, boron-doped float-zone silicon (FZ-Si) with thickness $t = (244 \pm 2)\,\mu$m and a doping concentration of $N_{\mathrm{dop}} = 1.5 \times 10^{16}\,\mathrm{cm}^{-3}$ ($1\,\Omega\,$cm) with a native oxide layer was used. After both-sided deposition of a hydrogen-rich SiN_x:H layer of thickness 200 nm in a PECVD process (reactive gases: SiH_4:NH_3 = 27 : 13; carrier gas: N_2; temperature 400 °C; duration per side: 240 s; PlasmaLab 100, Oxford Instruments; refractive index $n = 2.4$ at 632 nm), the sample was exposed to a rapid thermal treatment in a belt furnace with a measured peak temperature of 870 °C and a fast cool-down rate to introduce high amounts of hydrogen into the wafer mainly, but not exclusively in the form of dimers H_{2A}.

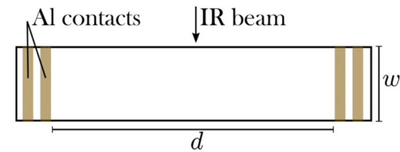

FIG. 1. Geometry of the sample suitable for both resistance and IR transmission measurements. In this study, an inner-terminal distance $d = 40$ mm and a width/optical path length $w = 10.6$ mm are used. The sample thickness is $t = 244\,\mu$m.

For highly sensitive four-point measurements as described elsewhere,[11] four stripe-like terminals were produced by thermal evaporation of aluminum and subsequent alloying through the SiN_x:H layer by laser pulses [laser fired contacts (LFCs)[18]] to provide a reliable and low-resistance contact. The wafer was broken in a stripe with a width (optical path length) of $w = 10.6$ mm revealing an optically smooth surface suitable for transmission measurements. Figure 1 illustrates the sample geometry, including the dimensions.

Resistance measurements were made with a digital multimeter (Keithley 2000, 6.5-digit) on a temperature stabilized measurement setup ($T = 25$ °C) as described elsewhere.[11]

The IR transmission spectra were obtained with a Vertex 80v FTIR-spectrometer from Bruker with a DLaTGS detector and a resolution $\Delta\tilde{\nu} = 3\,\mathrm{cm}^{-1}$. For the longitudinal measurements, the thin sample was clamped between two aluminum plates in order to detect only beam intensity that actually passes the sample. The interior of the spectrometer was extensively flushed with N_2 to suppress parasitic absorption, e.g., by water vapor. Each presented measurement was averaged 300 times (~20 min) to suppress noise.

Between each measurement, the sample was annealed at $T = 220$ °C in the dark on a hotplate to trigger formation and dissociation of BH pairs.

IV. DATA ANALYSIS

A. Resistance measurement

Due to its higher accuracy, direct contact resistance measurements were engaged to provide data on the change in hole concentration Δp. As explained in more detail elsewhere,[11] the electrical conductivity σ is dependent on BH pair concentration [BH] present in the p-type sample because it implies a deviation of hole p and doping concentration N_{dop},

$$\sigma = q \times \mu_p \times p = q \times \mu_p \times (N_{\mathrm{dop}} - [\mathrm{BH}]). \qquad (3)$$

Here, q denotes the elementary charge and μ_p the calculated hole mobility. Taking only the change in BH pair concentration $\Delta[\mathrm{BH}] = -\Delta p$ to a reference state $(R_0, \mu_{p,0})$ into account eliminates the necessity to know N_{dop} exactly. Therefore, $\Delta[\mathrm{BH}]$ is in the used geometry given by resistance R and thickness t of the sample as

© Author(s) 2022

well as width w and distance d of the Al contacts,

$$\Delta[\mathrm{BH}] = \frac{d}{q\,w\,t} \times \left(\frac{1}{\mu_{p,0}\,R_0} - \frac{1}{\mu_p\,R} \right). \quad (4)$$

B. Transmission data

The measured sample intensity I is lowered compared to the incident beam intensity I_0 due to three effects: shading of the beam due to the geometry of the specimen holder by a constant factor f_{geo} (which might differ between measurements due to inaccurate sample repositioning), reflection on the air/Si interface with the wavenumber-dependent reflectance $R(\tilde{\nu})$ and multiple internal reflections within the sample, and absorption of photons with the wavenumber-dependent total absorption coefficient $\alpha(\tilde{\nu})$ following Beer–Lambert's law with optical path length w. Therefore, the beam intensity after passing the sample is given by

$$I = f_{\mathrm{geo}} \times \frac{(1-R)^2\ \mathrm{e}^{-\alpha w}}{1 - R^2\ \mathrm{e}^{-2\alpha w}} \times I_0 \quad (5)$$

taking incoherent internal reflection into account.[19,20]

In the IR region studied here, absorption in the sample may occur by excitation of either local vibrational modes (LVMs) of impurities, such as BH (absorption coefficient α_{BH}), or the quasi-free electron gas (coefficient α_{Drude}) well-described by Drude's theory; hence, $\alpha = \alpha_{\mathrm{Drude}} + \alpha_{\mathrm{BH}}$. Both reflectance $R(n, k)$ and absorption coefficient $\alpha_{\mathrm{Drude}}(k) = 4\pi k\tilde{\nu}$ depend on the complex refractive index $\hat{n} = n + \mathrm{i}\,k = \sqrt{\varepsilon(\omega)}$, which in turn depends on the complex dielectric function $\varepsilon(\omega)$. Drude's theory states that permittivity (in the common circular frequency notation with $\omega = 2\pi c\tilde{\nu}$) for a quasi-free electron gas is given by

$$\varepsilon(\omega) = \varepsilon_\infty - \frac{\omega_{\mathrm{p}}^2}{\omega^2 + \mathrm{i}\,\omega/\tau}, \quad (6)$$

with ε_∞ being the static permittivity and τ being the scattering time. It also introduces the characteristic plasma frequency ω_{p},

$$\omega_{\mathrm{p}}^2 = \frac{q^2}{\varepsilon_0 \varepsilon_{\mathrm{r}} m} \times p, \quad (7)$$

which depends in our case on the hole concentration p and the effective hole mass m. It further comprises elementary charge q, relative permittivity of the host lattice ε_{r}, and vacuum permittivity ε_0. In summary, Drude's model can be used to describe reflectance R and α_{Drude}. In our case, with $p = 1.5 \times 10^{16}\,\mathrm{cm}^{-3}$, the plasma frequency is found to be in the range of $20\,\mathrm{cm}^{-1}$, allowing for approximations since the energy range regarded in this study is much higher. The function for the absorption coefficient α_{Drude} derived from Eq. (6) can thus be expanded so that the absorption can be described by

$$\alpha_{\mathrm{Drude}}(\tilde{\nu}) \approx \frac{\omega_{\mathrm{p}}^2}{\tilde{\nu}^2 \tau c} \sim \frac{p}{\tilde{\nu}^2}. \quad (8)$$

It turns out that $\alpha_{\mathrm{Drude}}(\tilde{\nu})$ varies noticeably with wavenumber $\tilde{\nu}$. Since k becomes small compared to n, $\hat{n} \approx n$ in this energy region. The refractive index n, however, has an insignificant dependency on wavenumber for $\omega \gg \omega_{\mathrm{p}}$, which can be seen by calculating the respective spectra. Therefore, the reflectance R is hardly affected by free-carrier absorption in this energy region.

The geometry factor f_{geo} was eliminated by comparison of the measured transmission to the calculated transmission applying Drude's theory on the data from resistivity measurements (p) and hole mobility μ_p,[21] the same for the reflectance R.

The total absorption coefficient was obtained from Eq. (5) and fitted taking a Gaussian shape of α_{BH} and the Drude background from Eq. (8) into account. By integrating the background corrected LVM-excitation α_{BH} or the quotient $\alpha_{\mathrm{BH}}/\tilde{\nu}$, the area can be normalized to the concentration known from the resistivity measurements, yielding two calibration factors depending on the procedure.

V. RESULTS AND DISCUSSION

A. Change in the charge carrier concentration

As a result of dark anneal, the resistance rises from its initial value and lowers again for treatment times above 5 h. The corresponding change in [BH] is depicted in Fig. 2. The fitted curve according to Eq. (2) perfectly describes the change, giving strong evidence for this effect to be caused by a change in BH pair concentration and matches results obtained by previous work.[9,11,22]

As described before, the change of free-carrier concentration p should impact the curvature of Drude absorption ($\alpha_{\mathrm{Drude}} \sim \omega_{\mathrm{p}}^2 \sim p$). Indeed, this can be confirmed as illustrated in Fig. 3, where the total wavenumber-dependent absorption coefficient $\alpha(t_i)$ for different times t_i during the dissociation of BH pairs is depicted. To better see the effect, the difference of the respective

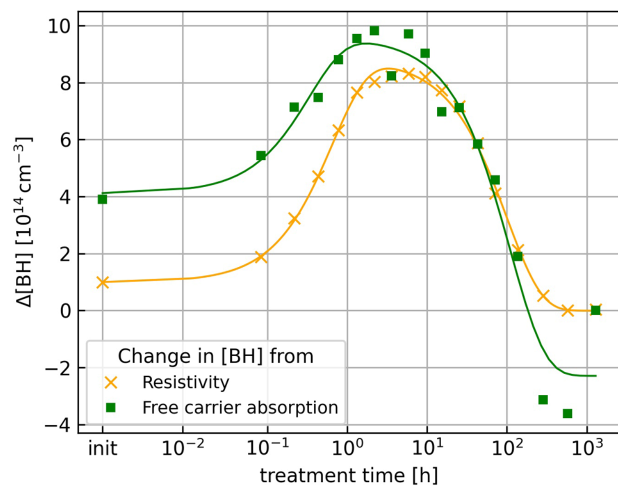

FIG. 2. Comparison of the change in boron–hydrogen pairs obtained by resistance measurements and calculated from free-carrier absorption in IR spectra. Both quantities use the long-term limit (at $t = 1300$ h) as a reference state.

© Author(s) 2022

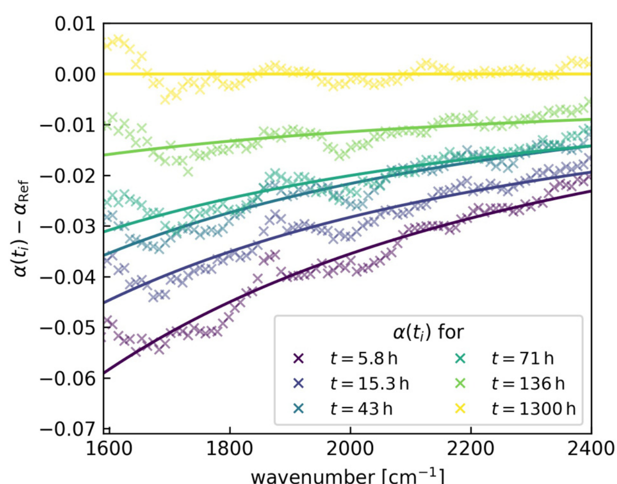

FIG. 3. Difference of absorption spectra for different times t_i and reference state $\alpha\,(t = 1300\,\text{h})$. The Drude absorption lowers with decreased hole concentration due to BH formation.

spectra $\alpha(t_i)$ and the absorption of the sample with minimum amount of BH pairs α_{Ref} at $t = 1300\,\text{h}$, i.e., the long-term limit, are shown in Fig. 3. Upon dissociation of BH pairs, the absorption is increased due to the increased hole concentration such that the curving is a measure for [BH] present in the sample.

Taking Eq. (8) into account, the corresponding change in [BH] is calculated by

$$\Delta[\text{BH}]_{\text{Drude}} = p_0 \times \left(1 - \frac{\alpha_{\text{Drude}}}{\alpha_{\text{Drude},0}}\right) \tag{9}$$

with respect to the reference state $\alpha_{\text{Drude},0}$ with hole concentration p_0 (obtained from resistivity measurements) at $t = 1300\,\text{h}$. The fitted Drude absorption [Eq. (8)] in the wavenumber range between 1600 and 2400 cm^{-1} was evaluated with Eq. (9), and the result of this evaluation is depicted in Fig. 2 in comparison with the values obtained by direct resistance measurements. There are inconsistencies between the two data sets. First, the evaluation by IR measurements seems to overestimate the initial BH concentration by about $3 \times 10^{14}\,\text{cm}^{-3}$. The reason for this significant deviation is difficult to find since a possible underlying effect would only occur at the initial measurement and would only affect the absorption by free charge carriers, but not the resistance. Second, according to Eq. (9), the evaluation relies on the last data point as a reference point. Due to the scatter of the individual measuring points along the fitting line, an uncertainty of this reference point must be assumed, which affects all other points.

B. LVM of BH pairs

To take advantage of bond-specific detection using IR spectra, the Drude part of the absorption coefficient has been subtracted. Therefore, the spectra depicted in Fig. 3 are fitted with a Drude $\text{const}/\tilde{\nu}^2$ function and a Gaussian peak function. All spectra have been fitted together with the same full-width of half maxima (FWHM $= 34\,\text{cm}^{-1}$). These background corrected absorption coefficients $\alpha_{\text{BH}} = \alpha - \alpha_{\text{Drude}}$ are depicted in Fig. 4 for different times t_i during a dark anneal at $T = 220\,°\text{C}$.

As can be seen, a peak is formed around $\tilde{\nu} = 1868\,\text{cm}^{-1}$. Its height and area increase until a total treatment time of $t = 5\,\text{h}$ and decreases again until it is no longer distinguishable from noise. This technique is thus able to reproduce the already known stretching mode of the boron–hydrogen complex[10,23,24] in a time-resolved manner during pair formation and resolution at room temperature. Contrary to previous work, this detection is not limited to highly doped layers[25] or requires low temperatures,[12,13] which allows for statements about the silicon bulk and frequent measurements (for example, during the annealing process). The advantage of

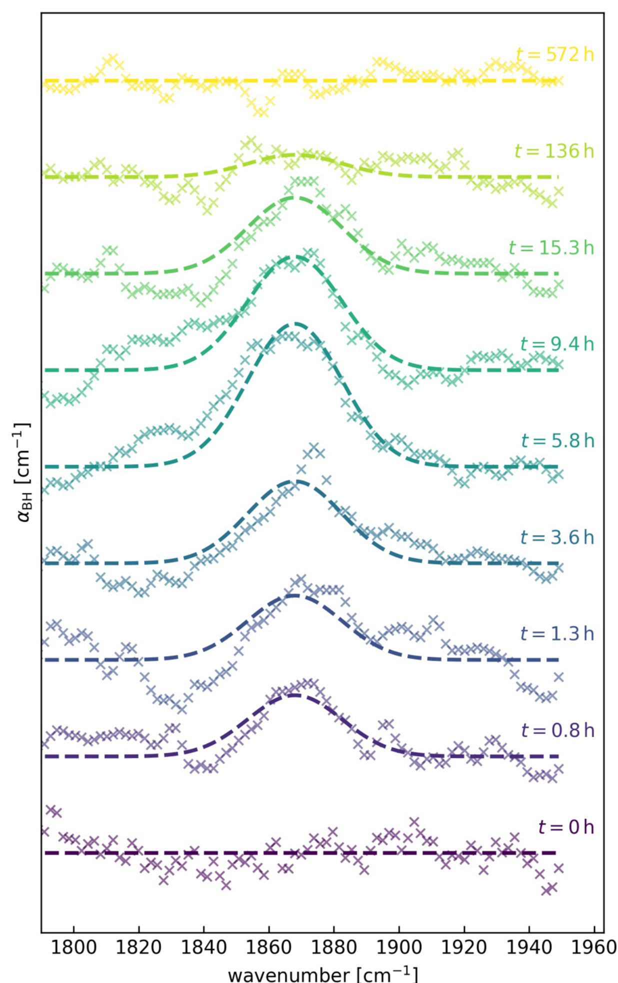

FIG. 4. Absorption coefficient α_{BH} for different stages during dark anneal at $T = 220\,°\text{C}$. Dotted lines are peak function fits (Gaussian) with FWHM $= 34\,\text{cm}^{-1}$. The spectra are shifted along the y axis for better visibility.

© Author(s) 2022

TABLE I. Calibration factors of integrated absorption coefficient α_{BH} (second column: $\alpha_{BH}/\tilde{\nu}$) and the BH pair binding concentration at room temperature for both commonly used denotations.

Definition	$[BH] = A^{\alpha}_{BH} \times \int \alpha_{BH}\, d\tilde{\nu}$	$[BH] = A^{\alpha/\tilde{\nu}}_{BH} \times \int \frac{\alpha_{BH}}{\tilde{\nu}}\, d\tilde{\nu}$
Calibration factor	$A^{\alpha}_{BH} = (4.2 \pm 0.3) \times 10^{15}\,cm^{-1}$	$A^{\alpha/\tilde{\nu}}_{BH} = (7.8 \pm 0.6) \times 10^{18}\,cm^{-2}$

measuring at room temperature is that the study of the BH complex can be coupled with the absorption by charge carriers to good agreement. This would not be possible at cryogenic temperatures since doping freezes out partially.

In addition, the sample design allows these measurements to be compared to high-precision resistance measurements. The proportionality between the integrated absorption coefficient of the LVM and the concentration of the respective binding is given by the equations depicted in Table I.[26–28] Since both the integrated α and the quotient $\alpha/\tilde{\nu}$ are commonly used in the literature, both equations have been evaluated in the following analysis.

The integrated absorption coefficient (quotient $\alpha/\tilde{\nu}$) can be normalized to Δ[BH] obtained by resistivity measurements. The maxima of fitted curves according to Eq. (2) were used as reference points since this is the best way to incorporate the different uncertainties of the single measurements. Uncertainties of transmission measurements were determined through evaluation of the uncertainty of the mean using Student's t-distribution on ten subsequent measurements for a constant BH concentration of $[BH] = 8 \times 10^{14}\,cm^{-3}$, which is used for the calculation of the calibration factors and their uncertainty. For this calculation, this is the most reasonable uncertainty since the calibration factor is also determined at this concentration. The respective value is depicted in Fig. 5 together with the uncertainty interval obtained by the fitting procedure. The determined uncertainty is in principle only valid for the concentration for which it was determined. The choice of an absolute value also for concentrations below $8 \times 10^{14}\,cm^{-3}$ overestimates the actual value. However, as the signal-to-noise ratio becomes worse with decreasing BH concentration, the relative uncertainty also increases, which means that the calculation of a relative uncertainty is also prone to error. However, the uncertainty of the calibration factor is determined only by the uncertainty for high concentrations. Since the error of BH pair concentration obtained via resistance measurements is below $10^{13}\,cm^{-3}$, it can be neglected here.[11]

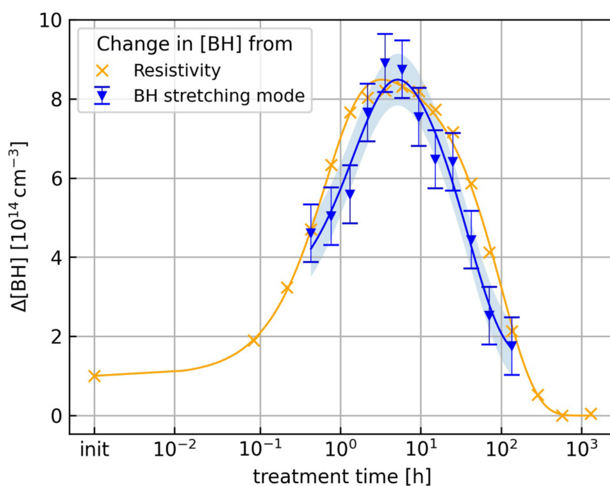

FIG. 5. Integrated absorption coefficient of the BH stretching mode in different stages during dark anneal compared to change in [BH] obtained from resistivity measurements. Lines are fits according to Eq. (2), including a 68% uncertainty range.

Thus, for the calibration factor between integrated α (quotient $\alpha/\tilde{\nu}$) and the concentration of the boron–hydrogen pair binding at room temperature, the values shown in Table I are determined.

VI. CONCLUSION

The absorption of the BH stretching mode at $1868\,cm^{-1}$ is detectable at room temperature, and the respective change due to BH pair formation and dissociation can be tracked. The detection limit is about $2 \times 10^{14}\,cm^{-3}$, and the uncertainty of the method presented here is about $1 \times 10^{14}\,cm^{-3}$. This direct evidence shows that changes in resistivity are indeed generated by BH pair formation/dissociation, making resistivity measurements sufficient to describe BH pairs. Since the measurements were performed at room temperature, this method allows investigations with little effort and standard laboratory equipment. IR transmission measurements reveal alterations in Drude absorption according to the change in the charge carrier concentration in agreement to resistivity and LVM analysis. This extension shows the consistency of the two chosen measurement methods and would not be possible at cryogenic temperatures because the doping would freeze out partially. The comparison between both types of analysis allows one to determine the calibration factor between the integrated absorption coefficient and the binding concentration at room temperature.

ACKNOWLEDGMENTS

The authors would like to thank Barbara Rettenmaier for technical support. Part of this work was supported by the German Federal Ministry of Economic Affairs and Climate Action under Contract No. 03EE0152A.

AUTHOR DECLARATIONS

Conflict of Interest

The authors have no conflicts to disclose.

© Author(s) 2022

DATA AVAILABILITY

The data that support the findings of this study and details on the measurement setup are available from the corresponding author upon reasonable request.

REFERENCES

[1] S. J. Pearton, J. W. Corbett, and T. S. Shi, "Hydrogen in crystalline semiconductors," Appl. Phys. A **43**, 153–195 (1987).

[2] M. A. Jensen, A. Zuschlag, S. Wieghold, D. Skorka, A. E. Morishige, G. Hahn, and T. Buonassisi, "Evaluating root cause: The distinct roles of hydrogen and firing in activating light- and elevated temperature-induced degradation," J. Appl. Phys. **124**, 085701 (2018).

[3] T. H. Fung, M. Kim, D. Chen, C. E. Chan, B. J. Hallam, R. Chen, D. N. Payne, A. Ciesla, S. R. Wenham, and M. D. Abbott, "A four-state kinetic model for the carrier-induced degradation in multicrystalline silicon: Introducing the reservoir state," Sol. Energy Mater. Sol. Cells **184**, 48–56 (2018).

[4] D. Chen, P. Hamer, M. Kim, C. Chan, A. Ciesla nee Wenham, F. Rougieux, Y. Zhang, M. Abbott, and B. Hallam, "Hydrogen-induced degradation: Explaining the mechanism behind light- and elevated temperature-induced degradation in n- and p-type silicon," Sol. Energy Mater. Sol. Cells **207**, 110353 (2020).

[5] J. Schmidt, D. Bredemeier, and D. C. Walter, "On the defect physics behind light and elevated temperature-induced degradation (LeTID) of multicrystalline silicon solar cells," IEEE J. Photovolt. **9**, 1497–1503 (2019).

[6] S. Jafari, U. Varshney, B. Hoex, S. Meyer, and D. Lausch, "Understanding light- and elevated temperature-induced degradation in silicon wafers using hydrogen effusion mass spectroscopy," IEEE J. Photovolt. **11**, 1363–1369 (2021).

[7] G. Hahn, A. Schönecker, A. R. Burgers, R. Ginige, K. Cherkaoui, and D. Karg, "Hydrogen kinetics in crystalline silicon–PECVD SiN studies in mc and Cz silicon," in *Proceedings of 20th European PV Solar Energy Conference and Exhibition* (WIP-Renewable Energies, 2005), pp. 717–720.

[8] D. C. Walter, D. Bredemeier, R. Falster, V. V. Voronkov, and J. Schmidt, "Easy-to-apply methodology to measure the hydrogen concentration in boron-doped crystalline silicon," Sol. Energy Mater. Sol. Cells **200**, 109970 (2019).

[9] C. Winter, J. Simon, and A. Herguth, "Study on boron–hydrogen pairs in bare and passivated float-zone silicon wafers," Phys. Status Solidi A **218**, 2100220 (2021).

[10] J. I. Pankove, P. J. Zanzucchi, C. W. Magee, and G. Lucovsky, "Hydrogen localization near boron in silicon," Appl. Phys. Lett. **46**, 421–423 (1985).

[11] A. Herguth and C. Winter, "Methodology and error analysis of direct resistance measurements used for the quantification of boron–hydrogen pairs in crystalline silicon," IEEE J. Photovolt. **11**, 1059–1068 (2021).

[12] P. M. Weiser, E. Monakhov, H. Haug, M. S. Wiig, and R. Søndenå, "Hydrogen-related defects measured by infrared spectroscopy in multicrystalline silicon wafers throughout an illuminated annealing process," J. Appl. Phys. **127**, 065703 (2020).

[13] M. Stavola, S. J. Pearton, J. Lopata, and W. C. Dautremont-Smith, "Vibrational characteristics of acceptor–hydrogen complexes in silicon," Appl. Phys. Lett. **50**, 1086–1088 (1987).

[14] M. Stavola and W. B. Fowler, "Tutorial: Novel properties of defects in semiconductors revealed by their vibrational spectra," J. Appl. Phys. **123**, 161561 (2018).

[15] M. Stavola, E. Elinor Chen, W. Beall Fowler, and G. Alvin Shi, "Interstitial H_2 in Si: Are all problems solved?," Physica B **340-342**, 58–66 (2003).

[16] R. E. Pritchard, J. H. Tucker, R. C. Newman, and E. C. Lightowlers, "Hydrogen molecules in boron-doped crystalline silicon," Semicond. Sci. Technol. **14**, 77–80 (1999).

[17] V. V. Voronkov and R. Falster, "Formation, dissociation, and diffusion of various hydrogen dimers in silicon," Phys. Status Solidi B **254**, 1600779 (2017).

[18] E. Schneiderlöchner, R. Preu, R. Lüdemann, and S. W. Glunz, "Laser–fired rear contacts for crystalline silicon solar cells," Prog. Photovolt.: Res. Appl. **10**, 29–34 (2002).

[19] M. H. Brodsky, M. Cardona, and J. J. Cuomo, "Infrared and Raman spectra of the silicon-hydrogen bonds in amorphous silicon prepared by glow discharge and sputtering," Phys. Rev. B **16**, 3556–3571 (1977).

[20] N. Maley, "Critical investigation of the infrared-transmission-data analysis of hydrogenated amorphous silicon alloys," Phys. Rev. B **46**, 2078–2085 (1992).

[21] PV Lighthouse, Mobility calculator; see https://www2.pvlighthouse.com.au/calculators/mobility%20calculator/mobility%20calculator.aspx.

[22] D. Bredemeier, D. C. Walter, R. Heller, and J. Schmidt, "Impact of hydrogen-rich silicon nitride material properties on light-induced lifetime degradation in multicrystalline silicon," Phys. Status Solidi RRL **13**, 1900201 (2019).

[23] M. Stavola, S. J. Pearton, J. Lopata, and W. C. Dautremont-Smith, "Vibrational spectroscopy of acceptor-hydrogen complexes in silicon: Evidence for low-frequency excitations," Phys. Rev. B **37**, 8313–8318 (1988).

[24] M. Stutzmann, "Hydrogen passivation of boron acceptors in silicon: Raman studies," Phys. Rev. B **35**, 5921–5924 (1987).

[25] D. Yong-Chang, Z. Yu-Feng, Q. Guo-Gang, and W. Shi-Fu, "Localized vibrational mode infrared absorption of BH pair in silicon," Solid State Commun. **55**, 501–503 (1985).

[26] P. G. Dawber and R. J. Elliott, "Theory of optical absorption by vibrations of defects in silicon," Proc. Phys. Soc. **81**, 453–460 (1963).

[27] R. Newman, "Infra-red absorption due to localized modes of vibration of impurity complexes in ionic and semiconductor crystals," Adv. Phys. **18**, 545–663 (1969).

[28] R. K. Willardson, E. R. Weber, and M. Stavola, *Identification of Defects in Semiconductors* (Academic Press, 1998).

© Author(s) 2022